A condensation origin for the mass-dependent silicon isotopic variations in Allende components: implications for complementarity

Rayssa Martins, Marc Chaussidon, Zhengbin Deng, Francesco C Pignatale, Frédéric Moynier

Earth and Planetary Science Letters ••• (••••) ••••••

A condensation origin for the mass-dependent silicon isotopic variations in Allende components: implications for complementarity

Rayssa Martins [1], Marc Chaussidon *, Zhengbin Deng [2], Francesco Pignatale, Frédéric Moynier

Université de Paris, Institut de physique du globe de Paris, CNRS, F-75005 Paris, France

ARTICLE INFO

Article history:
Received 16 April 2020
Received in revised form 28 October 2020
Accepted 10 November 2020
Available online xxxx
Editor: W.B. McKinnon

Keywords:
silicon isotopes
Allende chondrite
condensation
complementarity
chondrules

ABSTRACT

Primitive chondrites have bulk compositions close to that of the solar photosphere, with however significant variations of elemental ratio relative to the solar composition, depending on the volatility of the elements considered. This is classically understood as indicating a primary geochemical signature due to the formation of the components of chondrites (refractory inclusions, chondrules and matrix), or of their precursors, through condensation of a gas of near solar composition, plus secondary variations due to processes such as (i) incomplete volatilization of presolar components, (ii) complex high-temperature exchanges between condensed phases and the nebular gas, and (iii) sorting and transport of grains in the accretion disk before accretion of chondrite parent bodies. Because most of the mass of chondrites is made by elements which condense at high temperatures, equilibrium condensation produces in general little isotopic fractionation for these elements. Silicon is however an exception with per mil level equilibrium isotopic fractionation at high temperature between the SiO gas and condensed silicates, allowing to use silicon isotopes in chondrites to constrain the origin of their components and to put at test scenarios of condensation.

Individual components (chondrule fragments, isolated olivines in the matrix, and matrix fragments) of the carbonaceous chondrite Allende were separated and analysed at high-precision for their silicon isotopic composition. Large variations have been found among chondrules (δ^{30}Si from -0.86 ± 0.16‰ 2 s.e. to +0.04 ± 0.03‰ for 11 chondrules), isolated olivines (δ^{30}Si from -0.51 ± 0.12‰ 2 s.e. to +0.20 ± 0.10 ‰ for 12 olivines), and matrix (δ^{30}Si from -0.95 ± 0.08‰ 2 s.e. to -0.41 ± 0.01 ‰ for 17 matrix fragments). These variations distribute on both sides of the bulk δ^{30}Si value of Allende (-0.43 ± 0.03‰ 2 s.e., Armytage et al., 2011; Pringle et al., 2013, 2014; Savage and Moynier, 2013). There is a global positive trend between δ^{30}Si values and Mg/Fe ratio for chondrules and isolated olivines. This systematics appears in agreement with what can be modeled for producing Allende components, or their precursors, from fractionated condensation of a single gaseous reservoir having initially the silicon isotopic composition of bulk Allende. Mass balance taking into account the mean abundances and δ^{30}Si values of Allende components is consistent with their accretion in the Allende parent body in the proportions produced by the condensation of the parent parcel of nebular gas. This supports complementarity between chondrules, olivines and matrix as being a primary feature. However, this conclusion cannot be definitive because of the uncertainties in defining mean δ^{30}Si values for Allende components.

1. Introduction

During the formation of the solar System, most chemical elements were introduced in the accretion disk in the form of interstellar dust grains, the gaseous phase being made dominantly of a H_2 + CO gas with a fraction of other volatiles such as nitrogen or rare gases. Because high temperatures develop in the inner accretion disk due to radiative and viscous heating, the interstellar dust can be either vaporized, thermally processed or preserved, depending whether it is injected in the disk close or far from the

* Corresponding author.
E-mail address: chaussidon@ipgp.fr (M. Chaussidon).
[1] Present address: Department of Earth Science and Engineering, Imperial College London, London SW7 2AZ, UK.
[2] Present address: Centre for Star and Planet Formation, Globe Institute, University of Copenhagen, Denmark.

https://doi.org/10.1016/j.epsl.2020.116678

forming Sun (Pignatale et al., 2018). The components making primitive chondrites (Ca-, Al-rich inclusions or CAIs, chondrules and matrix) formed at various temperatures and times in the accretion disk (e.g. Scott and Krot, 2014). Their precursors can thus be considered to be either (for the major part) the products of the condensation of a gas made by vaporization of interstellar dust, or interstellar dust which escaped total evaporation and was variously processed or preserved in the accretion disk.

The facts that (i) primitive chondrites have bulk chemical compositions close to that of the solar photosphere with carbonaceous chondrites and more specifically CI chondrites having the best match (Lodders, 2003), and that (ii) the different chondrite groups show elemental fractionations relative to CI depending on temperature of condensation of the elements (Palme et al., 2014), are generally considered to indicate that the three major components of chondrites, or their precursors, formed from the condensation of a gas close to solar in composition. Carbonaceous chondrites are enriched in refractory elements and depleted in volatile elements. Among carbonaceous chondrites, the CV chondrites are the most fractionated with e.g. Al/Si ratio ≈1.4 times higher than CAI, Mg/Si ratio slightly higher than CI, and Na/Si ratio ≈0.5 times CI (Palme et al., 2014). The simplest interpretation of such a fractionation in chondrites would be to consider that it reflects various proportions of mixing between high-temperature and low-temperature (i.e. early and late) products of a condensation sequence. However, the real processes at play behind this fractionation have long been controversial (e.g. Anders, 1977; Wai and Wasson, 1977; Wasson, 1977). Recently, it was shown that mixing of four components (a CAI-like component, a chondrule-like component, an anhydrous matrix-like component, and water) could explain the diversity both in chemical fractionation and in non-mass-dependent isotopic compositions of carbonaceous chondrites (Alexander, 2019).

Most of the mass of condensable elements is made by O, Mg, Si and Fe: the Mg/Si ratio changes from 2 to 1 between forsterite and enstatite, predicted to condense sequentially from a solar gas (Grossman, 1972). In CV chondrites, the fact that the two major components hosting these elements (chondrules and matrix) have compositions (Mg/Si chondrules >Mg/Si CI > Mg/Si matrix) and proportions (45% vol for chondrules and 40% vol for matrix) resulting in a solar like bulk composition has led to the idea of chemical complementarity between chondrules and matrix (Hezel and Palme, 2010; Palme et al., 2015). This seems verified even at small scales, i.e. for masses of 600 mg in the Allende CV3 chondrite for instance (Palme et al., 2015). Complementarity means that matrix minerals are made from the total condensation of the parcel of gas remaining after the condensation and extraction of the precursors of the chondrules, or that matrix minerals formed from a gas processed by the formation of chondrules (e.g. Bland et al., 2005; Friend et al., 2016; Hezel et al., 2018 and refs therein). Thus, a key implication of complementarity is that matrix cannot have a CI composition, i.e. that of the initial gas. This has been observed but its real meaning has been challenged arguing that the non-CI composition of the matrix is a post-accretion secondary feature related to parent-body fluid-assisted chemical exchanges between chondrules and matrix (Zanda et al., 2018). In addition, the relative abundance of presolar grains and organic matter in the matrix of the most primitive chondrites is CI-like (Alexander, 2005). However, complementarity seems present in different classes of CV chondrites despite large variations in abundance and chemical compositions between matrix and chondrules between these classes (e.g. Hezel and Palme, 2010; Ebel et al., 2016).

Observed isotopic variations, either mass-dependent or non mass-dependent of nucleosynthetic origin, are not decisive regarding complementarity. Strontium isotopic variations ($^{88}Sr/^{86}Sr$ ratio) between chondrules (depleted in ^{88}Sr by up to ≈ -1.7‰) and matrix (enriched in ^{88}Sr by up to ≈ +0.7‰) observed in Allende has been interpreted as reflecting isotopic fractionation during fluid-assisted metamorphism on the parent body, but the light $^{88}Sr/^{86}Sr$ ratio of the CAIs was considered as primary and reflecting fractionation during either condensation or electromagnetic sorting of the partially ionized nebula gas (Moynier et al., 2010). Recent Zn isotopic data ($^{66}Zn/^{64}Zn$ ratio) on chondrules and matrix of the CV3.1 Leoville (Van Kooten and Moynier, 2019) revealed significant variations between the olivine-rich core of chondrules and their igneous rims (the cores being depleted in ^{66}Zn by ≈ -0.4‰) and between the matrix and the igneous rims of chondrules (the matrix being enriched in ^{66}Zn by ≈ 0.2‰). These variations are not interpreted as reflecting complementarity but as reflecting primarily Zn isotopic fractionations due to the presence of a sulfide immiscible melt during interactions between the nebula gas and the partially melted chondrules (Van Kooten and Moynier, 2019). At variance, chondrules and matrix in Allende appear complementary for their ^{183}W isotope anomalies (^{183}W depletion from -1.5 to -0.7 ppm in matrix, ^{183}W excess from +1.4 to +2.3 ppm in chondrules, and no anomaly in bulk) in agreement with their formation from a single reservoir of dust in which the presolar carriers of the ^{183}W anomalies were sorted between the precursors of chondrules and of matrix (Budde et al., 2016). Alternatively, it has been proposed that these variations in ^{183}W between chondrules and matrix could be due to the partial remobilization of W from chondrule to matrix during hydrothermal oxidation of chondrule metal-blebs (Alexander, 2019). Finally, the range of Fe isotopic variations of chondrules from Allende and from the CM chondrite Murchison (variations of the $^{56}Fe/^{54}Fe$ ratio from ≈ -0.6 to ≈ +0.4‰ around the bulk values of Allende and Murchison) is indicative of formation of the chondrules from a single reservoir from which the matrix also derives, with most of the isotopic variability due to pre-accretion evaporation/recondensation processes and not to post-accretion hydrothermalism and metasomatism (Mullane et al., 2005; Hezel et al., 2018). None of these isotopic studies, with the exception of Fe isotope studies, concern the major elements (O, Mg, Si) that represent the major mass of chondrules and matrix.

Here we present a high-precision Si isotope study of individual components in the CV3 chondrite Allende: single chondrules, Mg-rich olivines isolated in the matrix and bulk matrix samples. This study was designed to search for systematics in mass-dependent Si isotope variations among Allende components that could test and possibly further constrain (i) their origin by condensation processes from a single gaseous reservoir and (ii) their chemical and isotopic complementarity acquired by fractional condensation of this initial parent gaseous reservoir. Si isotopes show large mass-dependent equilibrium isotopic fractionations at high-temperature between SiO gas and silicate (e.g. $\Delta^{30}Si_{enstatite\text{-}gas}$ and $\Delta^{30}Si_{olivine\text{-}gas}$ increasing from ≈+1‰ to +2‰ with temperature decreasing from 2000 K to 1450 K, Clayton et al., 1978; Javoy et al., 2012; Méheut et al., 2009) so that during a condensation sequence the condensates and remaining gas will develop specific Si isotopic compositions. Allende was chosen because (i) it is a case study for complementarity (Hezel and Palme, 2010; Palme et al., 2015), (ii) existing Si isotopic data for the Ca-, Al-rich inclusions (Clayton et al., 1988; Grossman et al., 2008) and for chondrules and matrix (Armytage, 2011; Kadlag et al., 2018; Villeneuve et al., 2020) show the presence of large isotopic variations, (iii) the relative abundances of the various components have been recently redetermined (Ebel et al., 2016), and (iv) it is, among CV chondrites, the one richest in isolated Mg-rich olivines in the matrix that can thus be handpicked and analysed individually for Si isotope composition. Despite Allende being an oxidized CV of type >3.6 (Bonal et al., 2006), detailed chemical mapping shows that Si was not significantly redistributed by parent body processes between the different components (Ebel et al., 2016).

2. Methods

Chondrules, isolated olivines and matrix fragments were hand-picked from a roughly crushed fragment of the Allende CV3 chondrite. They were inspected microscopically and fragments were studied by scanning electron microscope (see supplementary for details). The isolated olivines, as well as the matrix samples and aliquots of the broken chondrules, were digested following NaOH fusion protocols modified after Georg et al. (2006). The glass cakes produced were dissolved in Milli-Q H_2O, and the solutions processed through cation exchange resin to purify Si (Pringle et al., 2014). These solutions were measured for Si isotopic compositions on a Neptune plus (Thermo-Fisher) multi-collector inductively-coupled-plasma mass spectrometer (MC-ICP-MS) at IPGP with procedures dedicated to minimize blanks and analytical errors for small sample mass (see supplementary for all analytical details). 92 runs of the NBS-28 standard solution at 2 ppm Si concentration yield a 2 s.d. of ± 0.13‰ and a 2 s.e. of ± 0.01‰ for δ^{30}Si values, where δ^{30}Si represents the per mil deviation of the $^{30}Si/^{28}Si$ ratio of the sample relative to that of NBS 28 standard.

3. Results

3.1. Range of Si isotopic variations

The 11 Allende chondrules analyzed show a large range of bulk Si isotopic variations with δ^{30}Si (where $\delta^{30}Si = [(R_{sample}/R_{NBS28}) - 1] \times 1000$; $R = ^{30}Si/^{28}Si$) from -0.86 ± 0.16‰ (2 s.e.) to +0.04 ± 0.03‰ (Table 1), in agreement with previous data (range for 10 Allende bulk chondrules from -0.71 ± 0.03 to -0.10 ± 0.03‰, Armytage, 2011). In situ analyses in Allende chondrules by femtosecond laser ablation coupled with MC-ICP-MS also show the presence of large Si isotopic variations from -1.28 ± 0.19‰ to +0.32 ± 0.19‰ (Kadlag et al., 2019). Even larger δ^{30}Si variations, from -3.41 ± 0.3‰ to +1.9 ± 0.3‰ were reported from ion microprobe in-situ analyses (at a spatial scale of ≈10 µm) of olivines in type I and type II chondrules (311 spots analysed in 17 chondrules) from Allende (Villeneuve et al., 2020; Fig. S4a). The 12 isolated Allende olivines studied show a range of variations for δ^{30}Si values from -0.51 ± 0.12‰ to +0.15 ± 0.10‰ (Table 1). This range is also lower than the range found from ion probe analyses in two Allende isolated olivines by Villeneuve et al. (2020) from -2.8 ± 0.3‰ to 0 ± 0.3 ‰ (17 spots in 2 isolated olivines, with however one spot at -4.5 ± 0.3‰).

At variance with bulk chondrules and isolated olivines, the 17 samples of matrix show a significantly more negative range of δ^{30}Si values from -0.95 ± 0.08‰ to -0.41 ± 0.01‰. The mean δ^{30}Si value for the matrix is of -0.65 ± 0.26‰ (2 s.d.). This is indistinguishable from the value of -0.63 ± 0.04‰ (2 s.e.) reported by Armytage (2011) for 17 analyses of a homogenized sample of Allende matrix. The present data show the presence of small but significant Si isotopic variations in the matrix. These variations, because of the matrix sampling procedure (see 2. Methods), cannot be attributed to the presence of visible fragments of chondrules, CAIs or isolated olivines. These variations are however much more restricted than the range of δ^{30}Si values from -1.33 ± 0.15‰ to +0.65 ± 0.21‰ found by in situ analyses in samples of matrix variously enriched in refractory or volatile elements (Kadlag et al., 2018).

3.2. Mass-dependent isotopic variations

Note that the present study was not designed to optimize precision on Δ^{29}Si but to optimize precision on δ^{30}Si for small samples. In a Si three-isotope diagram (Fig. 1), all the present Si isotopic variations appear mass-dependent within errors, except for one isolated olivine which has a marginally significant ^{29}Si deficit with $\Delta^{29}Si$ = -0.16‰ ± 0.10‰ (Δ^{29}Si being defined as $\delta^{29}Si - 0.517 \times \delta^{28}Si$). Some Allende CAIs are known to contain large Si isotope anomalies with Δ^{29}Si from -0.12 to +1.18‰ (7 among 26 CAIs studied in Clayton et al., 1988). These non-zero Δ^{29}Si values can be considered to reflect the presence within CAI precursors of presolar components carrying Si isotopic anomalies of nucleosynthetic origin. Thus, except for one sample, all the present Si isotopic variations reflect Si isotopic fractionations having taken place during the formation of matrix minerals, chondrules and isolated olivines, or of their precursors. If presolar components were present in their precursors, they must have been either vaporized or processed in the nebular gas at sufficiently-high temperatures to lose their initial Si isotopic signature. Studies of various kind of meteorites show that the presolar nebula in bulk did not contain any Si isotopic anomaly relative to the Earth within 15 ppm (e.g. Fitoussi et al., 2009; Zambardi et al., 2013; Pringle et al., 2013).

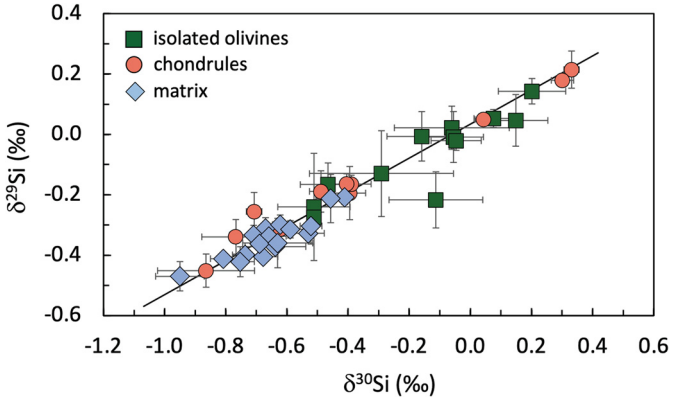

Fig. 1. Si three-isotope diagram for the present samples of Allende components. Errors shown are 2 s.e. Only one sample (of isolated olivine) shows a marginally significant non mass-dependent isotopic variation. All others samples define a δ^{29}Si versus δ^{30}Si line with a slope of 0.536 (+0.017/-0.035) consistent with the slope of the mass fractionation line (0.517). Note that isolated olivines have higher δ^{30}Si values than matrix, while chondrules distribute over the whole range of variations.

3.3. Systematics among Allende components

As shown in Fig. 2, all but two fragments of matrix have δ^{30}Si values lower than bulk Allende (-0.43 ± 0.10‰ 2 s.d., ± 0.03‰ 2 s.e., calculated for 10 different aliquots of Allende analysed in Armytage et al., 2011; Pringle et al., 2013, 2014; Savage and Moynier, 2013) while all isolated olivines (except 2) have δ^{30}Si values higher than the bulk. Chondrules have bulk δ^{30}Si values distributing above and below bulk Allende composition. Note that CAIs from CV chondrites (data from Clayton et al., 1988 and Grossman et al., 2008) have very variable δ^{30}Si values ranging from -1.77‰ to +5.96‰ (average of +1.42 ± 3.86 ‰), with 12 CAIs (out of the 28 CAIs with no Si isotopic anomaly) having δ^{30}Si values within 0 ± 1‰.

Despite some outliers, there is a broad trend between bulk δ^{30}Si values and Mg# (Mg#= 100×Mg/(Mg+Fe), with the Fe and Mg contents in atomic %, see Table S1) for isolated olivines and chondrules with δ^{30}Si values decreasing with decreasing Mg# (see Fig. 5). A similar trend seems present in the in-situ data by Kadlag et al. (2019). The present Mg-rich isolated olivines have systematically higher δ^{30}Si values (average of -0.03 ± 0.31‰ 2 s.d. for 9 olivines) than Fe-rich isolated olivines (average of -0.50 ± 0.05‰ 2 s.d. for 3 olivines, Table 1). Note that, in all chondrules but one, the Mg# of the olivines are higher than the Mg# of the bulk chondrule fragment (Table S1), so that the δ^{30}Si vs Mg# trend would be even better defined when considering isolated olivines and chondrule olivines together. Ion probe data by Villeneuve et al. (2020) show

Table 1
Silicon isotope data for Allende components.

Sample	Type	Mg#[a]	δ^{29}Si(‰)[b]	2 s.d.[c]	2 s.e.[d]	δ^{30}Si(‰)[b]	2 s.d.	2 s.e.	n[e]
AL19A1-10	Mg-rich olivine	96.2	-0.01	0.16	0.08	-0.16	0.23	0.11	4
AL19F1-5	Mg-rich olivine	97.2	0.05	0.17	0.09	0.15	0.21	0.10	4
AL19F2-1	Mg-rich olivine	96.9	0.02	0.14	0.07	-0.06	0.38	0.19	4
AL19F2-2	Mg-rich olivine	95.2	0.05	0.06	0.03	0.08	0.13	0.06	4
AL19G2-4	Mg-rich olivine	96.6	-0.13	0.28	0.14	-0.29	0.47	0.24	4
AL19I2-1	Mg-rich olivine	96.1	-0.01	0.17	0.08	-0.05	0.20	0.10	4
AL19K2-5	Mg-rich olivine	96.5	-0.02	0.06	0.03	-0.05	0.16	0.08	4
AL19L1-1	Mg-rich olivine	97.0	-0.22	0.19	0.09	-0.11	0.31	0.15	4
AL19N1-3	Mg-rich olivine	98.7	0.14	0.08	0.04	0.20	0.22	0.11	4
AL19D1-3	Fe-rich olivine	91.4	-0.24	0.35	0.18	-0.51	0.24	0.12	4
AL19E2-2	Fe-rich olivine	84.8	-0.17	0.14	0.07	-0.47	0.18	0.09	4
AL19G1-4	Fe-rich olivine	90.0	-0.27	0.11	0.05	-0.51	0.02	0.01	4
Ch3	Chondrule	80.2	-0.31	0.05	0.02	-0.62	0.04	0.02	4
Ch6	Chondrule	92.0	0.05	0.03	0.02	0.04	0.05	0.03	4
AL19CH-1	Chondrule	88.0	-0.19	0.18	0.09	-0.39	0.10	0.05	4
AL19CH-2	Chondrule	82.3	-0.34	0.11	0.06	-0.77	0.22	0.11	4
AL19CH-3	Chondrule	90.8	0.21	0.12	0.06	0.33	0.05	0.02	4
AL19CH-4	Chondrule	89.6	-0.16	0.06	0.03	-0.39	0.04	0.02	4
AL19CH-6	Chondrule	85.6	-0.19	0.14	0.07	-0.49	0.07	0.04	4
AL19CH-7	Chondrule	83.5	-0.26	0.13	0.06	-0.71	0.05	0.03	4
AL19CH-9	Chondrule	83.7	-0.16	0.07	0.03	-0.40	0.16	0.08	4
AL19CH-11	Chondrule	85.0	-0.45	0.11	0.05	-0.86	0.32	0.16	4
AL19CH-12	Chondrule	86.6	0.18	0.04	0.02	0.30	0.06	0.04	3
Mtx1	Matrix	51.0	-0.21	0.05	0.02	-0.41	0.03	0.01	4
Mtx2	Matrix	53.8	-0.21	0.16	0.08	-0.46	0.10	0.05	4
AL19MX-2	Matrix	50.2	-0.31	0.07	0.04	-0.67	0.04	0.02	4
AL19MX-3	Matrix	50.7	-0.40	0.07	0.03	-0.74	0.12	0.04	8
AL19MX-5	Matrix	51.2	-0.33	0.06	0.03	-0.71	0.16	0.08	4
AL19MX-7	Matrix	55.5	-0.41	0.03	0.01	-0.81	0.07	0.04	3
AL19MX-9	Matrix	55.2	-0.30	0.05	0.03	-0.62	0.04	0.03	3
AL19MX-10	Matrix	53.7	-0.40	0.02	0.02	-0.68	0.07	0.05	2
AL19MX-11	Matrix	54.6	-0.31	0.08	0.03	-0.59	0.16	0.06	7
AL19MX-12	Matrix	53.4	-0.34	0.08	0.03	-0.66	0.14	0.06	6
Al-Mtx-1	Matrix	n.d.[f]	-0.33	0.05	0.02	-0.53	0.10	0.05	4
Al-Mtx-2	Matrix	n.d.	-0.47	0.10	0.05	-0.95	0.16	0.08	4
Al-Mtx-3	Matrix	n.d.	-0.37	0.04	0.02	-0.64	0.17	0.10	3
Al-Mtx-4	Matrix	n.d.	-0.42	0.09	0.05	-0.75	0.08	0.05	3
Al-Mtx-5	Matrix	n.d.	-0.30	0.12	0.06	-0.52	0.07	0.04	4
Al-Mtx-7	Matrix	n.d.	-0.36	0.08	0.04	-0.69	0.02	0.01	4
Al-Mtx-8	Matrix	n.d.	-0.36	0.14	0.08	-0.63	0.20	0.11	3

[a] Mg# = 100 × Mg/(Mg+Fe), Mg and Fe contents in atomic %.
[b] $\delta^{X}Si = [(R_{sample}/R_{NBS28}) - 1] \times 1000$; $R = {}^{X}Si/{}^{28}Si$ and NBS28 the international reference standard.
[c] 2 s.d. = 2 standard deviation.
[d] 2 s.e. = 2 standard error on the mean.
[e] n = number of analyses for this sample.
[f] n.d. = not determined.

that δ^{30}Si variations are more pronounced in Mg-rich olivines than in Mg-poor olivines but no trend between δ^{30}Si and Mg# can be identified (see Fig. S3 for comparison between the mean δ^{30}Si values for chondrules from ion probe data and the present bulk δ^{30}Si values).

4. Discussion

4.1. Silicon isotopic variations expected from kinetic isotopic fractionation

Previous studies (analytical, experimental and theoretical) show that FUN-CAIs (fractionation and unidentified nuclear effects) and "normal" CAIs exhibit large bulk Si isotopic variations with several ‰ positive and negative variations of δ^{30}Si values likely due to kinetic isotopic fractionations during Si evaporation and condensation processes, respectively (e.g. Clayton et al., 1988; Grossman et al., 2008; Mendybaev et al., 2013; Richter et al., 2002). In these studies, equilibrium condensation is considered to have produced only sub-‰ level of Si isotopic variations in the precursors of refractory inclusions. Present data and previous data (Armytage, 2011; Kadlag et al., 2018) show that the range of bulk δ^{30}Si values in isolated olivines, chondrules and matrix is much more limited than in refractory inclusions. This argues against kinetic isotopic fractionation processes playing a dominant role to control the bulk Si isotopic composition of chondrules, isolated olivines and matrix.

However, the large δ^{30}Si heterogeneities (from -7‰ to +2.6‰) found by ion microprobe at the scale of ≈ 10 µm in type I chondrule olivines and low-Ca pyroxenes and in a few isolated olivines from carbonaceous chondrites have been interpreted to show that, locally in some objects, the effects of kinetic Si isotopic fractionations can be important (Villeneuve et al., 2020). This can be either via the presence of relict phases carrying kinetic light Si isotope enrichments such as olivines derived from amoeboid olivine aggregate refractory inclusions (AOAs have been shown to have δ^{30}Si values from ≈-9‰ to -1‰; Marrocchi et al., 2019b) or via Si kinetic isotopic fractionation between chondrule melts and the ambient gas (Villeneuve et al., 2020). Using Δ^{17}O values (tracing the ^{16}O-rich reservoir parent of AOAs; Krot et al., 2004) to identify in chondrules relict AOAs olivines with negative δ^{30}Si values shows that this would explain a minor fraction of δ^{30}Si variation in chondrules (specially in Allende). Most of the intra-chondrule variations is thus ascribed to Si kinetic isotopic fractionation during interactions between the ambient gas and chondrule melts (Villeneuve et al., 2020).

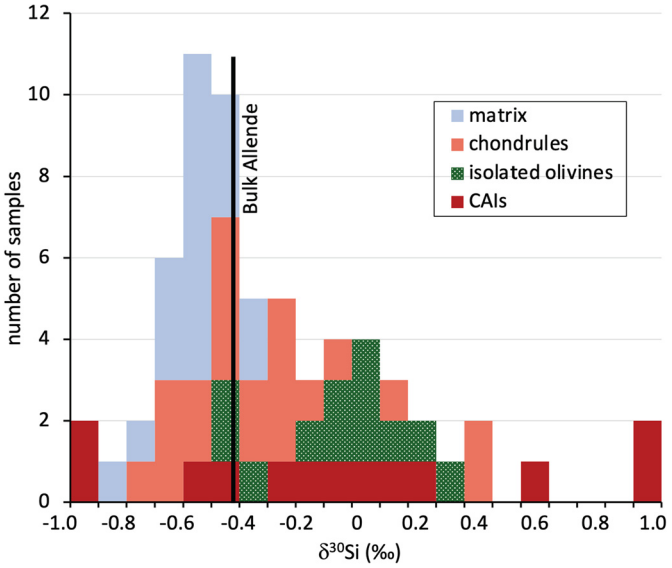

Fig. 2. Distribution of δ^{30}Si values among Allende components: isolated Mg-rich olivines from this study, chondrules from this study and from Armytage (2011), bulk Allende from Armytage et al. (2011), CAIs from Clayton et al. (1988) and from Grossman et al. (2008). To show the details of the δ^{30}Si variations in chondrules, isolated olivine and matrix, the scale was chosen from -1‰ to +1‰. Two CAIs with δ^{30}Si <-1‰ and 15 CAIs with δ^{30}Si >+1‰, among the 28 CAIs in Clayton et al. (1988) and Grossman et al. (2008) with no ^{29}Si anomaly (see text), are not shown. Similarly, AOAs olivines which have δ^{30}Si values from -9‰ to -1‰ (Marrocchi et al., 2019b) are not shown.

We note that, while kinetic Si isotope fractionation during condensation of olivines seems effectively the only viable explanation for the very low δ^{30}Si values of olivines from AOAs, this is not the only possible explanation of the δ^{30}Si heterogeneity in olivines from chondrules. This comes from the fact that Mg-rich olivines in AOAs are considered to have formed, probably in the CAIs forming region, by aggregation of high temperature condensates of CAI, metal and Mg-rich olivine (Krot et al., 2004). At these high-temperatures, the major reservoir of Si is still the SiO gas (e.g. Ebel and Grossman, 2000; Petaev and Wood, 2005) so despite significant equilibrium Si isotopic fractionation exists at high temperature (e.g. $\Delta^{30}Si_{olivine\text{-}SiO\ gas}$ = +1.6‰ at 1600K, Clayton et al., 1978; Javoy et al., 2012) no strong reservoir effect can be produced by condensation of olivines. For instance the removal of 20% of Si by the condensation of CAIs and olivines would decrease the δ^{30}Si of the remaining gas by only 0.4‰. This was pointed out early (Clayton et al., 1978). Thus, kinetic Si isotopic fractionation is definitely required to explain the light Si enrichments in AOAs olivines and this can constrain the duration of their condensation to be very short, days to weeks (Marrocchi et al., 2019b). The situation is very different for Fe-Mg chondrules which can be considered to have among their precursors Mg-Fe olivines and pyroxenes condensed at temperatures where a very small fraction of Si remains in the gas. At this stage, fractional equilibrium condensation can lead to large light Si enrichments in the last condensates: in fact, the distribution of in-situ δ^{30}Si values found by Villeneuve et al. (2020) is not better explained by kinetic isotopic fractionations during chondrule melting than by equilibrium isotopic fractionations during condensation of chondrule precursors (Figs S4a, b, c, d).

Thus, while it is clear that δ^{30}Si heterogeneity exists locally in chondrules and could result from non-equilibrium evaporation/condensation processes during chondrule formation, it is unlikely that they could have resulted in the systematic variations (tenths of ‰ of δ^{30}Si values, Fig. 2) among bulk isolated olivines, chondrules and matrix. In the next sections, we investigate how these bulk δ^{30}Si variations could result from simple equilibrium condensation of the silicate dust forming the precursors of chondrules and of the matrix.

4.2. Limited silicon isotopic variations expected from full equilibrium condensation

In the following we consider the Si isotopic evolution of a parcel of gas undergoing closed system full equilibrium condensation, to test if it can produce both the range of δ^{30}Si values observed in Allende components, and the broad relationship between Mg# and δ^{30}Si values of the condensates (Table 1). The equilibrium condensation sequence considers that within a parcel of gas, at any temperature during the condensation, the condensates are at chemical equilibrium with the gas (Grossman, 1972). In a canonical gas with solar composition and $P_{tot}=10^{-3}$–10^{-4} atm, thermodynamics shows that silicon begins to condense at around 1625 K in melilite ($Ca_2Al_2SiO_7$ gehlenite - $Ca_2MgSi_2O_7$ åkermanite solid solution) by reaction between the SiO gas and the Ca-Al-rich phases condensed at higher temperatures. Because the solar Al/Si and Ca/Si ratios are low (both <0.1), there is not enough Al and Ca available to condense all SiO from the gas. SiO is then removed from the gas at lower temperatures (between ≈1450 K and ≈1310 K) to form forsterite and enstatite by condensation and reactions with more refractory phases.

These temperatures of condensation can be significantly higher in case of condensation in non-canonical conditions. Dust-enriched systems have been considered (Palme and Fegley, 1990; Wood and Hashimoto, 1993; Ebel and Grossman, 2000) because they would allow to solve the discrepancy between the observation that high-temperature silicates in primitive chondrites have variable Mg/Fe ratios and the prediction that at high temperature in a canonical gas olivine and pyroxene are nearly pure forsterite and enstatite because Fe condenses as Fe-Ni metal (Grossman, 1972). Vaporizing silicate dust in dust-enriched systems makes the gas more oxidizing, thus stabilizing upon condensation silicates that can incorporate some Fe and that have Mg/Fe ratios decreasing with temperature (Ebel and Grossman, 2000). This effect is enhanced if water-rich CI dust is vaporized (Fedkin and Grossman, 2016). At a total pressure of 10^{-3} atm, the Mg# of olivine is predicted to decrease from 100 to 73% between 2000 and 1650 K for a dust enrichment of ×1000 and from 100 to 98% for a dust enrichment of ×100 (Ebel and Grossman, 2000). Thus, condensation in dust-enriched system predict Mg# similar to those observed in Allende chondrules and refractory olivines (Table 1), the first condensates (made at the highest temperature) being the most Mg-rich.

The condensates are expected to show significant Si isotopic variations because of the large equilibrium Si isotopic fractionation between silicate and SiO gas. The Si isotopic fractionation calculated from density functional theory (Javoy et al., 2012) between enstatite and SiO gas is given by:

$$\Delta^{30}Si_{enstatite\text{-}gas} = 4.1877 \times (10^6/T^2) - 0.056078 \times (10^6/T^2)^2 - 0.0002044 \times (10^6/T^2)^3 \quad (1)$$

implying that $\Delta^{30}Si_{enstatite\text{-}gas}$ increases from +1.58‰ to +2.42‰ for T decreasing from 1625 K to 1310 K. In this temperature range, no significant Si isotopic fractionation is expected between forsterite and enstatite with $\Delta^{30}Si_{forsterite\text{-}enstatite}$ ranging from -0.03 and -0.06 ‰ (Méheut et al., 2009). Calculations do not exist for refractory silicate phases such as melilite, but because in this temperature range Δ^{30}Si between silicates is expected to be 0 ± 0.3‰ (Clayton et al., 1978; Méheut et al., 2009; Javoy et al., 2012), it will be assumed in the following that $\Delta^{30}Si_{silicate\text{-}gas}$ = $\Delta^{30}Si_{enstatite\text{-}gas}$ during condensation.

The Si isotopic composition of the bulk silicate condensate can be calculated from simple mass balance of Si isotopes. In case of

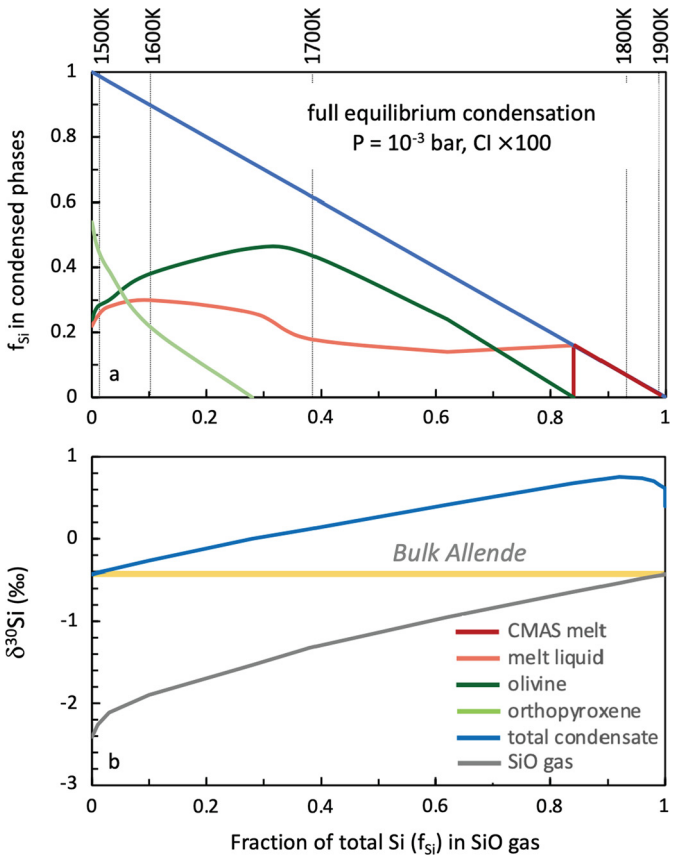

Fig. 3. Model for a condensation sequence at full equilibrium in a dust-enriched system (×100 enrichment in CI dust) for a total pressure of 10^{-3} bar. Fig. 3a: fractions of total Si in CaO-MgO-Al_2O_3-SiO_2 (CMAS) liquid, MELT liquid, olivine, orthopyroxene and total condensate versus fraction of Si in the SiO gas (data from Ebel and Grossman, 2000). Fig. 3b: Si isotopic composition of the total condensate and of the SiO gas versus fraction of Si in the SiO gas, assuming full isotopic equilibrium between the two phases (see text, Si isotopic fractionation from Javoy et al., 2012). Dashed lines show temperatures in K (from Ebel and Grossman, 2000). The yellow line shows the δ^{30}Si value of bulk Allende (-0.43‰) which is assumed to be that of the initial gas. (For interpretation of the colours in the figure(s), the reader is referred to the web version of this article.)

full isotopic equilibrium between the condensed phases and the SiO gas, at any temperature during the condensation sequence, mass balance is given by:

$$\delta^{30}Si_0 = f_{Si} \times \delta^{30}Si_{gas} + (1 - f_{Si}) \times (\Delta^{30}Si_{silicate-gas} + \delta^{30}Si_{gas}) \quad (2)$$

with f_{Si} the fraction of Si remaining in the SiO gas at this temperature, $\Delta^{30}Si_{silicate\text{-}gas}$ the equilibrium Si isotopic fractionation between silicate condensate and SiO gas at this temperature (assumed to be $\Delta^{30}Si_{enstatite\text{-}gas}$), and $\delta^{30}Si_0$ the Si isotopic composition of the SiO gas at the beginning of condensation (when f_{Si}=1). Bulk carbonaceous chondrites show little variations in δ^{30}Si values with an average of -0.48 ± 0.10‰ (2 s.d.; Armytage et al., 2011), the bulk δ^{30}Si value of Allende being of -0.43 ± 0.10‰ (2 s.d.; Armytage et al., 2011; Pringle et al., 2013, 2014; Savage and Moynier, 2013).

Taking this value of -0.43‰ for the initial Si isotope composition of the SiO gas, the δ^{30}Si values of the equilibrium silicate condensates can be calculated in a canonical nebula or in a dust-enriched system. In a canonical condensation sequence (Grossman, 1972), condensates will show δ^{30}Si values decreasing from +1.13‰ to -0.43‰ for temperatures from 1625 K (taking f_{Si}=0.99) to 1310 K (taking f_{Si}=0), respectively. At variance, for condensation in a dust-enriched system (Ebel and Grossman, 2000), f_{Si} decreases from 1 at T >≈ 2200 K to ≈ 0.38 at T ≈ 1700 K (for dust enrichment ×100) or to 0.45 at T ≈ 1950 K (for dust enrichment ×1000) (Fig. 3a and S5a). Thus, the high-temperature condensate will have positive δ^{30}Si values from ≈+0.42‰ for the first condensates to +0.12 ‰ at 1700 K (dust enrichment ×100), (or -0.06 ‰ at 1950 K for dust enrichment ×1000, see Figs. 3b and S5b). The difference in δ^{30}Si of the silicates for a similar f_{Si} for different dust enrichments is due to the change of $\Delta^{30}Si_{silicate\text{-}gas}$ with temperature.

By definition of mass balance, when f_{Si}=0, the δ^{30}Si value of the total condensate is $\delta^{30}Si_0$. Thus, if full isotopic equilibrium is maintained between the condensates and the gas, the δ^{30}Si values lower than -0.43‰ observed in chondrules, isolated olivines and the matrix cannot result from isotopic fractionation during condensation. Note also, that the presence of CAIs or a range in δ^{30}Si values among chondrules and isolated olivines are inconsistent with full equilibrium condensation.

4.3. Large silicon isotopic variations expected from fractional condensation

If equilibrium is not maintained between the condensed phases and the gas, the condensation is fractional. This can arise either from condensation with timescales shorter than those required for re-equilibration of solids with the gas by diffusion, or from simple removal of solids from the gas by e.g. vertical settling of the dust in the disk. In terms of chemical and isotopic mass balance, these two processes are equivalent. Pignatale et al. (2016) calculated a simple case of fractionation in three steps of a canonical solar gas (with $P_{tot}=10^{-3}$ atm and solar composition) during a classical condensation sequence. In this model, refractories with iron and minor silicates condensed between 1850 K (f_{Si}=1) and 1443 K (f_{Si}=0.88) are first fractionated at 1443 K, iron with forsterite and minor silicates condensed between 1443 K and 1380 K (f_{Si}=0.55) are fractionated at 1380 K, and the silicates condensed at lower temperature are enstatite with a minor amount of forsterite. From mass balance and (1), the δ^{30}Si values of the phases sequentially fractionated can be calculated to decrease from +1.4‰ for the minor silicates fractionated at 1443 K, to +0.5‰ for the forsterite fractionated at 1380 K, and finally to a range from +0.5‰ to -1.7‰ for the enstatite condensates fractionated below 1380 K. Obviously, such a fractional condensation produces a δ^{30}Si range corresponding to the range observed in Allende components (Fig. 2).

However, as explained in the previous section, condensation in dust-enriched systems would be required to explain the range observed for both δ^{30}Si values and Mg#. Calculations by Ebel and Grossman (2000) show that, upon condensation, the Mg# of condensed silicates and f_{Si} will decrease together with temperature, thus predicting a positive correlation between δ^{30}Si values and Mg#. First order predictions can be made for Si isotopic variations during fractional condensation using the approach of condensation with isolation (Petaev and Wood, 1998, 2005). In Petaev and Wood (1998) a single parameter is used to quantify the fraction of solids that are fractionated (or isolated): the isolation degree (ξ) simply defined as the percentage per Kelvin of condensed solids withdrawn from further reaction with the residual gas at lower temperature. Fractional condensation can be modeled for the two cases studied above (P_{tot} = 10^{-3} atm and dust enrichments of ×100, ×1000; Ebel and Grossman, 2000) by considering that a fraction of CAIs is isolated from the CMAS melt (f_{CAIs}= ξ × f_{CMAS}) and that a fraction of silicate is isolated from the silicates at equilibrium with the silicate melt (MELT) and the gas ($f_{Sil\text{-}isol}$= ξ × $f_{Sil\text{-}eq}$, subscripts Sil-isol and Sil-eq referring to isolated silicates and equilibrium silicates, respectively). During condensation, the

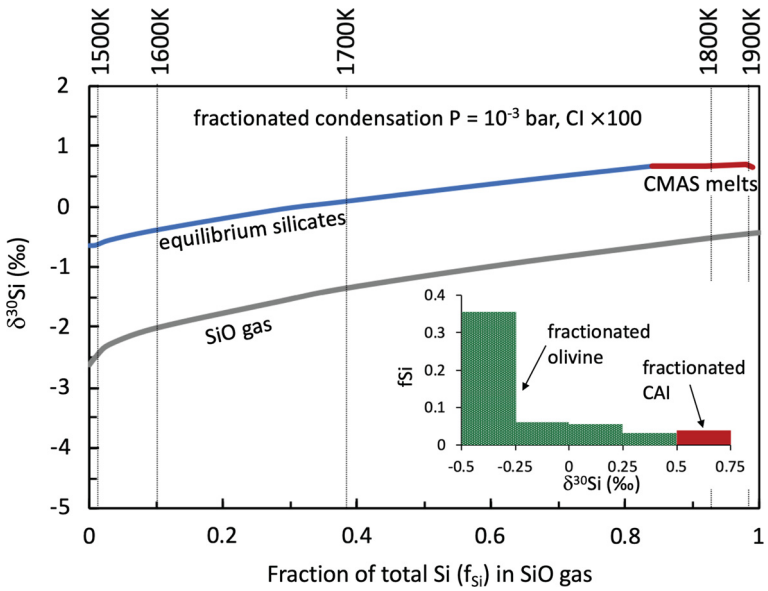

Fig. 4. Model for a condensation sequence with isolation (ξ=0.25%/K, see text) in a dust-enriched system (×100 enrichment in CI dust; Ebel and Grossman, 2000) for a total pressure of 10^{-3} bar. The curves show how the δ^{30}Si of the phases at equilibrium (in red the melt of CMAS composition, in blue all the equilibrium silicates, i.e. melt and crystals) with the SiO gas (grey curve) change with decreasing temperature during condensation. The insert is a histogram showing the fraction of total Si hosted by the isolated (or fractionated) solids (CAIs and olivines) versus their δ^{30}Si values. Dashed lines show temperatures in K (from Ebel and Grossman, 2000).

δ^{30}Si values of the SiO gas and of the phases condensed (at equilibrium or isolated) can be calculated at any step (i) of temperature drop from the δ^{30}Si values at step (i-1) and the following mass balance equation:

$$\delta^{30}Si_0 = f^i_{Si} \times \delta^{30}Si^i_{gas} + (f^i_{CMAS} + f^i_{MELTS} + f^i_{Sil-eq}) \times (\Delta^{30}Si^i_{silicate-gas} + \delta^{30}Si^i_{gas}) + \sum_{x=0}^{i-1} f^x_{CAI} \times \delta^{30}Si^x_{CAI} + \sum_{x=0}^{i-1} f^x_{Sil-isol} \times \delta^{30}Si^x_{Sil-isol}, \quad (3)$$

with f^i_A and $\delta^{30}Si^i_A$ the fractions of Si in phase A and its δ^{30}Si value at step (i), $\Delta^{30}Si^i_{silicate-gas}$the equilibrium Si isotopic fractionation between silicate and gas at the temperature corresponding to step (i). Fig. 4 shows the results for ξ = 0.25%/K and dust enrichment of ×100 (see Fig. S6 for ξ = 0.25%/K and dust enrichment of ×1000). This value of 0.25%/K for ξ is required to reach at the end of the condensation a low δ^{30}Si value for the equilibrium condensates of -0.64‰ that is similar to the bulk δ^{30}Si value of Allende matrix (the lowest bulk δ^{30}Si value of Allende components). When f_{Si}=0, the equilibrium condensates host 47.2% of all the Si condensed, while 3.4% is in the isolated CAIs and 49.4% in the isolated silicates (Fig. 4). A value of 0.25%/K for ξ is also required for dust enrichments of ×1000 to get a δ^{30}Si value -0.65‰ at the end of condensation, but the fractions of Si hosted in the different phases are slightly different (7.6% in isolated CAIs, 32.6% in isolated silicates, 59.8% in equilibrium silicates; Fig S6). In both cases, the isolated CAIs show the highest δ^{30}Si values (from +0.65‰ to +0.70‰ for dust enrichment ×100, Fig. 4) while the isolated silicates show a large range of δ^{30}Si values (from +0.41‰ to -0.43‰ for dust enrichment ×100, Fig. 4). The covariation of Mg# and δ^{30}Si values predicted by the model for condensed phases is shown in Fig. 5 for different values of ξ (0, 0.1, 0.25%/K).

Note that in this model of fractionated condensation for Si isotopes it is assumed that the phase diagram and phase compositions calculated for full equilibrium condensation by Ebel and Grossman (2000) are still valid. This is of course incorrect because, if a phase is fractionated from the condensation sequence to prevent re-equilibration of its Si isotopic composition with the SiO gas, the chemical composition of the bulk remaining system would be modified. This would possibly change phase relationships and compositions for the following part of the condensation sequence when isolation degree ξ >0.20%/K (Petaev and Wood, 1998). It is, however, beyond the scope of the present study to model that in detail. Anyway, due to the large Si isotopic variability of Allende components, the trend between δ^{30}Si and Mg# (Fig. 5) is not defined precisely enough to be matched to a unique condensation scenario. Note in addition that the oxidation state of the gas (controlled by the enrichment factor in CI dust and possibly water ice) is the major control of Mg# value of the total condensate at a given temperature (Fig. 5).

Thus, the range of bulk Si isotopic compositions observed in Allende isolated olivines, chondrules and matrix can result from the fractionated condensation of a gas having initially the silicon isotopic composition of bulk Allende. This range is caused by (i) reservoir effects for Si and by (ii) changes with temperature of the equilibrium Si isotopic fractionation between silicates and SiO gas. The model predicts, that the most refractory silicates will have positive δ^{30}Si values and that less refractory ones will have lower δ^{30}Si values. An isolation degree ξ of 0.25%/K is required to explain the low δ^{30}Si values of the less refractory silicates. This yields a fraction of Si condensed in CAIs (from 3.4% to 7.6%) consistent with observation in Allende (3.8% in CAIs and 2.1% in AOAs; Table 2; Ebel et al., 2016). The large fraction of Si condensed in isolated silicates (from 32.6% to 49.4%) is also consistent with the prevalence in Allende and CV chondrites of type I (Mg-rich) chondrules (Scott and Krot, 2014) containing in many cases relict Mg-rich olivines which escaped re-equilibration with the surrounding gas during the last chondrule melting event (e.g. Chaussidon et al., 2008; Rudraswami et al., 2011; Marrocchi et al., 2019a, and refs therein). Finally, the large fraction of Si condensed in equilibrium silicates (from 47.2% to 59.8%) is in agreement with the observations that a large fraction of olivines in type I chondrules are formed at near-equilibrium with the surrounding gas, as implied by their complex zoning and texture (Libourel and Portail, 2018) and by demonstrated gas-melt exchanges (Tissandier et al., 2002; Libourel et al., 2006; Marrocchi and Chaussidon, 2015; Friend et al., 2016; Barosch et al., 2019). Note that, at the larger scale of the disk, fractionation of olivine from the gas was proposed to be responsible of silicon isotopic

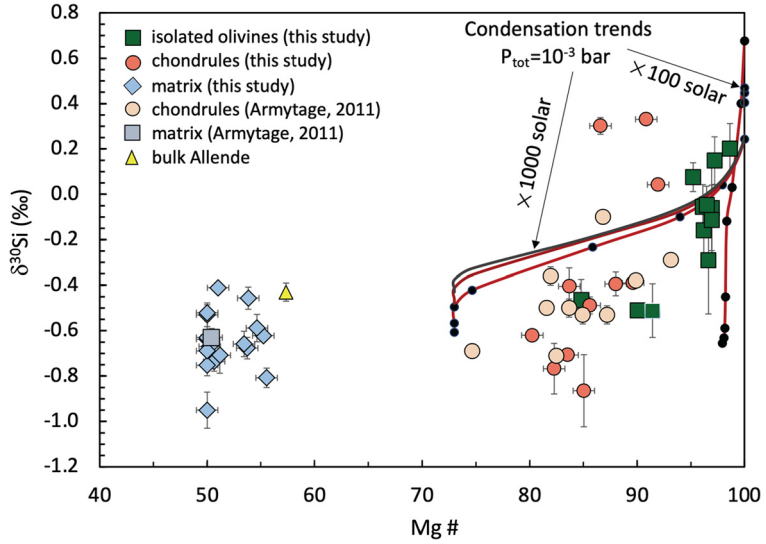

Fig. 5. Variations of the Si isotopic composition of isolated olivines, chondrules, and matrix versus their Mg# (data from this study and from Armytage, 2011). The bulk δ^{30}Si value of Allende is calculated from data in Armytage et al., 2011; Pringle et al., 2013, 2014; Savage and Moynier, 2013. Note that the general trend of decrease of δ^{30}Si values with decreasing Mg# (between 100 and ≈75) is broadly consistent with predictions made for the models of a condensation sequence with isolation of phases in dust-enriched systems as described in Fig. 4 for ×100 enrichment and in Fig. S6 for ×1000 enrichment. Each dot on the two condensation trends (calculated for isolation degree ξ = 0.25%/K) corresponds to increments of temperature of 50 K from minimum temperature of 1650 K (for ×100 enrichment) and of 1450 K (for ×1000 enrichment). For dust enrichment ×1000, the two other curves correspond to condensation trends calculated for ξ=0.10%/K and ξ=0%/K (upper curve, corresponding to the case of equilibrium condensation). For dust enrichment ×100, curves for ξ=0.25, 0.1 and 0%/K are mostly superimposed.

Table 2
Si distribution and isotopic compositions among Allende components.

Component	fraction total Si[a]	δ^{30}Si	2 s.d.	2 s.e.
CAIs	0.038	1.42[b]	3.86	0.73
AOAs	0.021	n.d.	n.d.	n.d.
Isolated olivines	0.017	-0.15[c]	0.52	0.16
Al-rich chondrules	0.025	n.d.	n.d.	n.d.
Chondrules	0.351	-0.41[d]	0.64	0.14
Matrix	0.548	-0.65[e]	0.25	0.06
Bulk Allende		-0.43[f]	0.10	0.03

[a] Fraction of total Si from Ebel et al. (2016). The fraction of Si hosted by isolated olivines is calculated from their abundance and SiO_2 contents assuming an average Mg# of 0.95.

[b] Average of the 28 out of 36 CAIs from Clayton et al. (1988) and Grossman et al. (2008) that have no large Si isotope anomaly (Δ^{29}Si<0.1‰).

[c] Average of the isolated olivines from this study that have no Si isotope anomaly (11 out of 12 analysed).

[d] Average of 21 chondrules (11 from this study and of 10 from Armytage (2011)).

[e] Average of 17 samples of matrix from this study and of 1 from Armytage (2011).

[f] Calculated for 10 different aliquots of Allende analysed in Armytage et al., 2011; Pringle et al., 2013, 2014; Savage and Moynier, 2013.

variations among planetary objects (Dauphas et al., 2015). Finally, the low Mg# and δ^{30}Si values of the matrix silicates can be explained by the predominance in the matrix of silicates condensed at lower temperatures than the precursors of chondrules and by the presence in the matrix of metal condensed together with the silicates (Ebel and Grossman, 2000). Mg-Fe exchange between matrix silicates and metal grains at lower temperature will not change the δ^{30}Si signature acquired by the silicates during condensation.

4.4. Silicon isotopic complementarity between Allende components

Allende components would be truly complementary for Si isotopes if they were present in Allende with the δ^{30}Si values and the proportions modeled for a fractional condensation sequence (see 4.3.). This would imply that they were accreted in relative abundances equal to that produced by the condensation sequence. Note that, even if CAIs precursors and chondrule precursors derive from different parent reservoirs (as suggested for instance from their different ^{16}O enrichments), they are predicted to show the same systematics for δ^{30}Si values as predicted in the previous section because (i) no significant δ^{30}Si variations are anticipated in the accretion disk (Armytage et al., 2011) and (ii) the condensation sequence would be similar in different reservoirs.

The mean δ^{30}Si values of the Allende components are possibly consistent with predictions made for fractional condensation from a gaseous reservoir having initially the bulk δ^{30}Si of Allende (see Figs. 4, 5 and previous section). Thus, one way to test the complementarity for Si isotopes is to verify that the bulk δ^{30}Si value measured for Allende is the same as calculated from the mean δ^{30}Si values predicted from fractional condensation for the different components. If not, this could indicate either (i) that the mean δ^{30}Si value used for one or several components is not correct, or (ii) that the components are not derived from a single reservoir having the δ^{30}Si value of bulk Allende. In both cases, Allende components would not be truly complementary for Si isotopes. There appears to be several limitations in making this exercise.

The first limitation is that Allende components show a range of δ^{30}Si values making the definition of a mean δ^{30}Si for each component difficult. This is exemplified by CAIs which show the largest range of δ^{30}Si variations, from -1.77‰ to +14.26‰ for the 36 CAIs from Clayton et al. (1988) and Grossman et al. (2008). This range is reduced but still large, from -1.77‰ to +5.96‰ (mean of +1.4 ± 3.9 ‰ 2 s.d., Table 1), if considering only the CAIs with small Δ^{29}Si anomalies (<0.1‰). The CAIs having large Si isotope anomalies (with a mean δ^{30}Si value of +4.7‰; Clayton et al., 1988) most likely formed from a mix of precursors containing many presolar grains which were not totally evaporated. Thus, they are not really relevant for testing condensation. Because of their small fraction (27% of all CAIs) and of the small fraction of total Si hosted in all CAIs (3.8%, Table 2), the contribution of CAIs to bulk Allende is not dominant. For instance, the bulk δ^{30}Si calculated for Allende would increase by 0.14‰ only if taking a mean δ^{30}Si value for CAIs of +5‰ instead of the value of +1.4‰ corresponding to the mean of "normal" CAIs. One way to understand this mean δ^{30}Si value of +1.4‰ (Table 2) is to consider that it represents the mean value

of CAIs precursors produced at the beginning of the condensation sequence (predicted to range from +0.2‰ to +0.7‰ if the starting gas has a δ^{30}Si of -0.43‰, see Fig. 4 and Fig. S6) modified by the kinetic isotopic fractionations due to evaporation and condensation during the complex re-heating history of CAIs and their precursors (e.g. Mendybaev et al., 2013; Richter et al., 2002; Richter, 2004; Grossman et al., 2008).

The second limitation comes from the fact that the δ^{30}Si values of AOAs have not been studied precisely in Allende. Though AOAs host a small fraction of total Si (2.1%), this represents however around twice more Si than "anomalous" CAIs. In addition, their δ^{30}Si values could be very negative as shown by recent ion microprobe data from three CV, CO and CM chondrites (Kaba, MIL 07342 and NWA 5958, respectively) showing a δ^{30}Si range for 69 individual olivine grains in 7 AOAs from -9.7±0.5‰ (2 s.d.) to -1.0±0.2‰ and an average δ^{30}Si value for the 7 AOAs of -4.3±1.7‰ (Marrocchi et al., 2019b). Using -4.3‰ instead of +1.4‰ (the value of "normal" CAIs) decreases the bulk δ^{30}Si value calculated for Allende by 0.12‰.

Bearing in mind these limitations, a bulk δ^{30}Si value of -0.55 ± 0.13‰ can be calculated for the sum of all the components listed in Table 2 using a value of -4.3‰ for AOAs (Marrocchi et al., 2019b) and assuming that normal chondrules and Al-rich chondrules share the same average δ^{30}Si value. This value seems consistent within errors with the bulk δ^{30}Si value of -0.43 ± 0.03‰ for Allende. Note that the δ^{30}Si value for the sum of Allende components would be even closer to the bulk of Allende if using for AOAs the mean δ^{30}Si value of CAIs: this would give a δ^{30}Si value of -0.43 ± 0.13‰. To make this test as stringent as possible we used the smallest possible error on the δ^{30}Si of the sum of Allende components, i.e. the 2 s.e. errors on the mean δ^{30}Si values of each component (Table 2). If considering in addition an error on the fraction of Si hosted by each component, or if taking 2 s.d. errors on δ^{30}Si values of the components instead of 2 s.e., the test would of course be verified but not really significant anymore because of the very large errors.

5. Conclusions

The silicon isotopic variations present among Allende components are consistent with resulting from a sequence of condensation. In such a scenario, early (CAIs and chondrule precursors, isolated olivines) and late (matrix minerals) condensates have δ^{30}Si values higher and lower than the initial gas, respectively, and are accreted together in more or less the proportions issued from the condensation sequence. This results in the bulk δ^{30}Si of Allende being that of the initial gas.

The fact that the different Allende components appear complementary relative to the condensation process for a major element such as Si, which has a 50% condensation temperature of 1310 K (Lodders, 2003), does not mean that complementarity is obligatorily verified for highly refractory or highly volatile elements. However, because it implies that all the major Allende components were accreted more or less in the proportions in which they (or their precursors) were produced by condensation, it is very likely that complementarity may also be observed for other elements that were fractionated between early-condensed and late-condensed phases.

CRediT authorship contribution statement

MC, FM and ZD designed the project. FM provided samples for study. RMP prepared the samples and performed the SEM study. ZD and RMP developed the technique, did the isotopic analyses, reduced the data and produced sample description and data tables. FP advised on condensation calculations. MC, FM, ZD, RMP and FP participated to the interpretation of the data. MC conceived and realized the model. ZD and RMP wrote the description of the analytical techniques. MC wrote the rest of the paper.

Declaration of competing interest

The authors declare that they have no known competing financial interests or personal relationships that could have appeared to influence the work reported in this paper.

Acknowledgements

This work was supported by ANR-15-CE31-0004-1 (ANR CRADLE), the UnivEarthS Labex program at Sorbonne Paris Citè (ANR-10-LABX-0023 and ANR-11-IDEX-0005-02) and the Région Île-de-France through the DIM-ACAV+ project "HOC - Origine de l'eau et du carbone dans le Système Solaire". Parts of this work were supported by IPGP multidisciplinary program PARI, and by Region île-de-France SESAME Grant (no. 12015908). We thank Andrew M. Davis and Dominik Hezel for their reviews and helpful comments.

Appendix A. Supplementary material

Supplementary material related to this article can be found online at https://doi.org/10.1016/j.epsl.2020.116678.

References

Alexander, C.M.O'D., 2005. Re-examining the role of chondrules in producing the elemental fractionations in chondrites. Meteorit. Planet. Sci. 40, 943–965.
Alexander, C.M.O'D., 2019. Quantitative models for the elemental and isotopic fractionations in chondrites: the carbonaceous chondrites. Geochim. Cosmochim. Acta 254, 277–309.
Anders, E., 1977. Critique of "Nebular condensation of moderately volatile elements and their abundances in ordinary chondrites" by Chien M. Wai and John T. Wasson. Earth Planet. Sci. Lett. 36, 14–20.
Armytage, R.M.G., 2011. The silicon isotopic composition of inner solar system materials. Unpublished PhD thesis. University of Oxford. 212 p.
Armytage, R.M.G., Georg, R.B., Savage, P.S., Williams, H.M., Halliday, A.N., 2011. Silicon isotopes in meteorites and planetary core formation. Geochim. Cosmochim. Acta 75, 3662–3676.
Barosch, J., Hezel, D.C., Ebel, D.S., Friend, P., 2019. Mineralogically zoned chondrules in ordinary chondrites as evidence for open system chondrule behaviour. Geochim. Cosmochim. Acta 249, 1–16.
Bland, P.A., Alard, O., Benedix, G.K., Kearsley, A.T., Menzies, O.N., Watt, L.E., Rogers, N.W., 2005. Volatile fractionation in the early solar system and chondrule/matrix complementarity. Proc. Natl. Acad. Sci. 103, 13755–13760.
Bonal, L., Ouirico, E., Bourot-Denise, M., Montagnac, G., 2006. Determination of the petrologic type of CV3 chondrites by Raman spectroscopy of included organic matter. Geochim. Cosmochim. Acta 70, 1849–1863.
Budde, G., Kleine, T., Kruijer, T.S., Burkhardt, C., Metzler, K., 2016. Tungsten isotopic constraints on the age and origin of chondrules. Proc. Natl. Acad. Sci. 113, 2886–2891.
Chaussidon, M., Libourel, G., Krot, A.N., 2008. Oxygen isotopic constraints on the origin of magnesian chondrules and on the gaseous reservoirs in the early Solar System. Geochim. Cosmochim. Acta 72, 1924–1938.
Clayton, R.N., Mayeda, T., Epstein, S., 1978. Isotopic fractionation of silicon in Allende inclusions. In: Proc. Lunar. Planet. Sci. Conf. 9th, pp. 1267–1278.
Clayton, R.N., Hinton, R.W., Davis, A.M., 1988. Isotopic variations in the rock-forming elements in meteorites. Philos. Trans. R. Soc. Lond. A 325, 483–501.
Dauphas, N., Poitrasson, F., Burkhardt, C., Kobayashi, H., Kurosawa, K., 2015. Planetary and meteoritic Mg/Si and δ^{30}Si variations inherited from solar nebula chemistry. Earth Planet. Sci. Lett. 427, 236–248.
Ebel, D.S., Grossman, L., 2000. Condensation in dust-enriched systems. Geochim. Cosmochim. Acta 64, 339–366.
Ebel, D.S., Brunner, C., Konrad, K., Leftwich, K., Erb, I., Lu, M., Rodriguez, H., Crapster-Pregont, E.J., Friedrich, J.M., Weisberg, M.K., 2016. Abundance, major element composition and size of components and matrix in CV, CO and Acfer 094 chondrites. Geochim. Cosmochim. Acta 172, 322–356.
Fedkin, A.V., Grossman, L., 2016. Effects of dust enrichments on oxygen fugacity of cosmic gases. Meteorit. Planet. Sci. 51, 843–850.
Fitoussi, C., Bourdon, B., Kleine, T., Oberli, F., Reynolds, B.C., 2009. Si isotope systematics of meteorites and terrestrial peridotites: implications for Mg/Si fractionation in the solar nebula and for Si in the Earth's core. Earth Planet. Sci. Lett. 287, 77–85.

Friend, P., Hezel, D.C., Mucerschi, D., 2016. The conditions of chondrule formation, part II: open system. Geochim. Cosmochim. Acta 173, 198–209.
Georg, R.B., Reynolds, B.C., Frank, M., Halliday, A.N., 2006. New sample preparation techniques for the determination of Si isotopic compositions using MC-ICPMS. Chem. Geol. 235, 95–104.
Grossman, L., 1972. Condensation in the primitive solar nebula. Geochim. Cosmochim. Acta 36, 597–619.
Grossman, L., Simon, S.B., Rai, V.K., Thiemens, M.H., Hutcheon, I.D., Williams, R.W., Galy, A., Ding, T., Fedkin, A.V., Clayton, R.N., Mayeda, T., 2008. Primordial compositions of refractory inclusions. Geochim. Cosmochim. Acta 72, 3001–3021.
Hezel, D.C., Palme, H., 2010. The chemical relationship between chondrules and matrix and the chondrule matrix complementarity. Earth Planet. Sci. Lett. 294, 85–93.
Hezel, D.C., Wilden, J.S., Becker, D., Steinbach, S., Wombacher, F., Harak, M., 2018. Fe isotope composition of bulk chondrules from Murchison (CM2): constraints for parent body alteration, nebula processes and chondrule-matrix complementarity. Earth Planet. Sci. Lett. 490, 31–39.
Javoy, M., Balan, E., Méheut, M., Blanchard, M., Lazzeri, M., 2012. First-principles investigation of equilibrium isotopic fractionation of O- and Si-isotopes between refractory solids and gases in the solar nebula. Earth Planet. Sci. Lett. 319–320, 118–127.
Kadlag, Y., Tatzel, M., Frick, D.A., Becker, H., Kühne, P., 2018. Chondrule-matrix complementarity in the Allende CV3 chondrite – a Si perspective. In: Lunar Planetary Science Conference. #1092 (abstract).
Krot, A.N., Petaev, M.I., Russel, S.S., Itoh, S., Fagan, T.J., Yurimoto, H., Chizmadia, L., Weisberg, M.K., Komatsu, M., Ulyanov, A.A., Keil, K., 2004. Amoeboid olivine aggregates and related objects in carbonaceous chondrites: records of nebular and asteroid processes. Chem. Erde 64, 185–239.
Libourel, G., Krot, A., Tissandier, L., 2006. Role of gas–melt interaction during chondrule formation. Earth Planet. Sci. Lett. 251, 232–240.
Libourel, G., Portail, M., 2018. Chondrules as direct thermochemical sensors of solar protoplanetary disk gas. Sci. Adv. 4 (7), eaar3321.
Lodders, K., 2003. Solar system abundances and condensation temperatures of the elements. Astrophys. J. 591, 1220–1247.
Marrocchi, Y., Euverte, R., Villeneuve, J., Batanova, V., Welsch, B., Ferrière, L., Jacquet, E., 2019a. Formation of CV chondrules by recycling of amoeboid olivine aggregate-like precursors. Geochim. Cosmochim. Acta 247, 121–141.
Marrocchi, Y., Chaussidon, M., 2015. A systematic for oxygen isotopic variation in meteoritic chondrules. Earth Planet. Sci. Lett. 430, 308–315.
Marrocchi, Y., Villeneuve, J., Jacquet, E., Piralla, M., Chaussidon, M., 2019b. Rapid condensation of the first solar system solids. Proc. Natl. Acad. Sci. 116, 23461–23466.
Méheut, M., Lazzeri, M., Balan, E., Mauri, F., 2009. Structural control over equilibrium silicon and oxygen isotopic fractionation: a first-principles density-functional theory study. Chem. Geol. 258, 28–37.
Mendybaev, R.A., Richter, F.M., Georg, R.B., Janney, P.E., Spicuzza, M.J., Davis, A.M., Valley, J.W., 2013. Experimental evaporation of Mg- and Si-rich melts: implications for the origin and evolution of FUN CAIs. Geochim. Cosmochim. Acta 123, 368–384.
Moynier, F., Agranier, A., Hezel, D.C., Bouvier, A., 2010. Sr stable isotope composition of Earth, the Moon, Mars, Vesta and meteorites. Earth Planet. Sci. Lett. 300, 359–366.
Mullane, E., Russell, S.S., Gounelle, M., 2005. Nebular and asteroidal modification of the iron isotope composition. Earth Planet. Sci. Lett. 239, 203–218.
Palme, H., Fegley Jr., B.J., 1990. High-temperature condensation of iron-rich olivine in the solar nebula. Earth Planet. Sci. Lett. 101, 180–195.
Palme, H., Hezel, D.C., Ebel, D.S., 2015. The origin of chondrules: constraints from matrix composition and matrix-chondrule complementarity. Earth Planet. Sci. Lett. 411, 11–19.
Palme, H., Lodders, K., Jones, A., 2014. Solar system abundances of the elements. In: Holland, H.D., Turekian, K.K. (Eds.), second edition. Treatise on Geochemistry, Vol. 2. Elsevier, Oxford, pp. 15–36.
Petaev, M.I., Wood, J.A., 1998. The condensation with partial isolation (CWPI) model of condensation in the solar nebula. Meteorit. Planet. Sci. 33, 1123–1137.
Petaev, M.I., Wood, J.A., 2005. Meteoritic constraints on temperatures, pressures, cooling rates, chemical compositions, and modes of condensation in the solar nebula. In: Krot, A.N., Scott, E.R.D., Reipurth, B. (Eds.), Chondrites and the Protoplanetary Disk. In: ASP Conferences Series, vol. 341, pp. 373–406.
Pignatale, F.C., Maddison, S.T., Liffman, K., Brooks, G., 2016. 2D condensation model for the inner solar nebula: an enstatite-rich environment. Mon. Not. R. Astron. Soc. 457 (2), 1359–1370.
Pignatale, F.C., Charnoz, S., Chaussidon, M., Jacquet, E., 2018. Making the planetary material diversity during the early assembling of the solar system. Astrophys. J. 867, L23–L27.
Pringle, E.A., Savage, P.S., Badro, J., Barrat, J.-A., Moynier, F., 2013. Redox state during core formation on asteroid 4-Vesta. Earth Planet. Sci. Lett. 373, 75–82.
Pringle, E.A., Moynier, F., Savage, P.S., Badro, J., Barrat, J.-A., 2014. Silicon isotopes in angrites and volatile loss in planetesimals. Proc. Natl. Acad. Sci. 111, 17029–17032.
Richter, F.M., 2004. Timescales determining the degree of kinetic isotope fractionation by evaporation and condensation. Geochim. Cosmochim. Acta 68, 4971–4992.
Richter, F.M., Davis, A.M., Ebel, D.S., Hashimoto, A., 2002. Elemental and isotopic fractionation of type B calcium-, aluminum-rich inclusions: experiments, theoretical considerations, and constraints on their thermal evolution. Geochim. Cosmochim. Acta 66, 521–540.
Rudraswami, N.G., Ushikubo, T., Nakashima, D., Kita, N.T., 2011. Oxygen isotope systematics in the Allende CV3 chondrite: high precision ion microprobe studies. Geochim. Cosmochim. Acta 75, 7596–7611.
Savage, P.S., Moynier, F., 2013. Silicon isotopic variation in enstatite meteorites: clues to their origin and Earth-forming material. Earth Planet. Sci. Lett. 361, 487–496.
Scott, E.R.D., Krot, A.N., 2014. Chondrites and their components, in meteorites and cosmochemical processes. In: Holland, H.D., Turekian, K.K. (Eds.), Treatise on Geochemistry Second Edition, Vol. 1. Elsevier, pp. 65–137.
Tissandier, L., Libourel, G., Robert, F., 2002. Gas–melt interactions and their bearing on chondrule formation. Meteorit. Planet. Sci. 37, 1377–1389.
Van Kooten, E., Moynier, F., 2019. Zinc isotope analyses of singularly small samples (<5 ng Zn): investigating chondrule-matrix complementarity in Leoville. Geochim. Cosmochim. Acta 261, 248–268.
Villeneuve, J., Marrocchi, Y., Jacquet, E., 2020. Silicon isotopic composition of chondrule silicates in carbonaceous chondrites and the formation of primordial solids in the accretion disk. Earth Planet. Sci. Lett. 542, 116318.
Wai, C.M., Wasson, J.T., 1977. Nebular condensation of moderately volatile elements and their abundances in ordinary chondrites. Earth Planet. Sci. Lett. 36, 1–13.
Wasson, J.T., 1977. Reply to Edward Anders: A discussion of alternative models for explaining the distribution of moderately volatile elements in ordinary chondrites. Earth Planet. Sci. Lett. 36, 21–28.
Wood, J.A., Hashimoto, A., 1993. Mineral equilibrium in fractionated nebular systems. Geochim. Cosmochim. Acta 57, 2377–2388.
Zambardi, T., Poitrasson, F., Corgne, A., Méheut, M., Quitté, G., Anand, M., 2013. Silicon isotope variations in the inner solar system: implications for planetary formation, differentiation and composition. Geochim. Cosmochim. Acta 121, 67–83.
Zanda, B., Lewin, E., Humayun, M., 2018. The chondritic assemblage. In: Russell, S., Connolly Jr., H., Krot, A. (Eds.), Chondrules: Records of Protoplanetary Disk Processes. Cambridge University Press, Cambridge, pp. 122–150.